ANTIPROTON DRIVEN MAGNETICALLY INSULATED INERTIAL CONFINEMENT FUSION (MICF) PROPULSION SYSTEM

NIAC 98-02 Final Report

By

Dr. Terry Kammash
Principal Investigator
Department of Nuclear Engineering and Radiological Sciences
The University Of Michigan
Ann Arbor, MI 48109
Tel: (734) 764-0205
Fax: (734) 763-4540
Email: tkammash@umich.edu

Abstract

        A comprehensive model of the plasma dynamics in MICF and how that translates
into the propulsive capability of the system was developed in this Phase I research effort.
Using the fundamentals of plasma physics, the time evolution of a fusion plasma
generated in a spherical pellet by an incident laser or particle beam is followed from
initiation to termination for the purpose of calculating that all important quantity known
as the "fusion gain factor Q". The higher the gain, the larger the energy content of the
plasma at the end of the burn, and the larger is the velocity of the plasma particles as they
emerge through the magnetic nozzle to produce the thrust. The main feature that
distinguishes MICF from other inertial fusion systems is the self-generated magnetic field
that serves to thermally insulate the plasma from the metal shell that physically contains
it during the burn. Such a field is shown to scale directly with the square root of the
plasma temperature and inversely with the spot diameter at the point of beam incidence,
and its decay time has a direct bearing on the plasma lifetime in the system. The
confinement time is determined by the time it takes the shock wave, initiated at the inner
surface of the metal shell at the time of beam incidence, to traverse the thickness of this
shell. Since the speed of sound varies directly with the square root of the temperature of
the medium and inversely with the square root of its density, its value in MICF is much
smaller than in "implosion-type" inertial fusion due to the larger atomic mass of the shell,
and its lower temperature that arises from the thermal insulation provided by the
magnetic field. A set of coupled, time dependent particle and energy balance equations
for all species in a multi-region target that includes the core plasma, the partially ionized
fuel region separated from the core by the magnetic field, and a metal shell divided
appropriately into three regions is solved to generate the gain factor. The solution
accounts for particle and energy transport across the magnetic field in both directions,
and for radiation transport from the core to the outer regions. Particles and energy
diffusion across the field that includes classical and anomalous transport were
incorporated in the analysis where it is shown that mild turbulence results in large gains
that can be attributed to a more efficient fueling by this process. Gains ranging from
several hundreds to several thousands are found to be feasible in MICF depending on the
target design and the incident energy. A nanogram of antiprotons is shown to be
sufficient to ignite a typical MICF target and, in a propulsion system, this could generate
a specific impulse of about a million seconds and a thrust of more than 10^4 Newtons if a
rep rate of 10 Hertz is used. These propulsive capabilities are considered crucial for
interstellar and some interplanetary missions.

        An additional objective of the phase I research is the generation of data that can
be used in designing targets for the purpose of conducting experiments in a phase II work
plan that will validate the theory and analysis carried out in phase I. With minor
modifications, the equations developed for a reactor can be used to predict the plasma
dynamics in a target with a fuel that generates little or no fusion energy, e.g., DD at a
relatively low temperature but capable of producing detectable magnetic fields upon
illumination by carefully chosen laser and/or particle beams such as energetic protons. It
will also allow for measurements of confinement time and other relevant signatures such
as neutron production which can be sizable even at modest temperatures. The eventual
utilization of antiprotons to produce meaningful plasma in MICF targets must await the

construction of traps for these particles currently under development at NASA's Marshall Space Flight Center.

1.0   Introduction

1.1   Executive Summary

NASA's challenges of interplanetary manned missions in the early part of the next century along with robotic interstellar missions such as the so-called "precursor mission" to the Oort Cloud at 10,000 AU in less than 50 years require propulsion systems that can produce specific impulses in the $10^5 - 10^6$ seconds range and thrusts in the tens to hundreds of kilonewtons. This automatically eliminates from consideration conventional propulsion systems and some of the advanced concepts such as nuclear thermal and gas core fission systems due to the small specific impulses they produce. With pure antimatter annihilation propulsion still very far in the future, fusion reactions with the next largest energy production per unit mass ($\sim 10^{14}$ J/kg) offer the most promising approaches to this challenge. Of particular interest is the antiproton-driven Magnetically Insulated Inertial Confinement Fusion (MICF) Concept because of its capability of meeting these demanding requirements and simultaneously lending itself to a near-term development due to current understanding of its underlying physics principles.

The Magnetically Insulated Inertial Confinement Fusion (MICF) Concept combines the favorable aspects of both magnetic and inertial fusion in that physical containment of the plasma is provided by a metallic shell such as tungsten or gold, while its thermal energy is insulated from that shell by a self-generated magnetic field. Fusion reactions in this device can be triggered by laser or particle beams that enter the target pellet through a hole to ablate the fuel-coated inner wall and form a hot plasma. The lifetime of such a plasma is dictated by the time it takes the shock wave initiated at the time of beam incidence to traverse the shell's thickness. This is estimated to be typically about 100 nanoseconds which is two orders of magnitude longer than "implosion" type inertial fusion, and that translates into longer fusion burn and greater energy multiplication. In a propulsion system, it is envisioned that MICF pellets injected into a reaction chamber will be zapped by a beam of antiprotons to initiate the fusion reactions and subsequently allowing the reaction products to exhaust through a magnetic nozzle to produce the desired thrust. This study has shown on the basis of established plasma physics laws that such a propulsion system has the capability of opening up revolutionary NASA mission scenarios for future interplanetary and interstellar spacecraft. The unique features of this concept with regard to future space travel opportunities are:

- The ability to generate very large fusion energy gains that translate into specific impulses on the order of a million seconds.
- The ability to capitalize on present day technology in the manufacture of fusion fuel-coated targets currently used in inertial fusion research for terrestrial power.
- The flexibility in target design to meet specific mission requirements. This can be accomplished by varying the proportions of the fusion fuel and the metal shell to

increase either the specific impulse or the thrust, i.e., to make the propulsion system a variable specific impulse, variable thrust device.

- The potential of making a low mass, comparatively low cost system that can be run by a small amount of antiprotons as opposed to massive and complicated laser drivers or particle drivers that require larger accelerators.
- The ability to generate large thrusts ($\sim 10^4 - 10^5$ Newtons) by careful selection of rep rates which in turn could allow a 10,000 AU mission to be accomplished in less than 50 years.

Some assumptions were employed in the analysis carried out in phase I which lead to the conclusions cited above. They must, however, be validated through experimentation to be proposed in phase II. These include:

- Verification of the generation of large magnetic fields in MICF targets.
- The scaling of these fields with plasma properties, and with target and incident-beam properties.
- Minimization of plasma loss through the hole through which the incident beam enters.
- In the absence of availability of antiprotons in the near future, the response of these targets to, say, proton beams of average energy of ~ 1 MeV.
- The degree and methods of focusing needed for such particle beams to enter the small holes in the tiny pellets.
- Identification of the particle transport across the magnetic field within the pellet, whether classical or anomalous, and the conditions that may enhance or inhibit each.
- Identification and/or discovery of unexpected phenomena that may impact the propulsive capability and performance of an MICF propulsion system.

1.2   Background and Rational

In recent years, NASA has set a number of challenging and ambitious mission goals for space exploration in the early part of the next century. These include manned missions to Mars in several months instead of several years, and some robotic interstellar missions to 10,000 AU in less than 50 years. As pointed out earlier, most of these interplanetary and interstellar missions require propulsion systems that can deliver specific impulses in the range of $10^5 - 10^6$ seconds and thrusts in the tens to hundreds of kilonewtons. These are the very parameters that distinguish current from future propulsion systems and as Fig. 1 reveals, that classification is a meaningful and an informative one. If one adopts a simply trajectory consisting of a continuous burn acceleration/deceleration at a constant thrust for such missions, then it can be readily shown from the standard non-relativistic rocket equation that the round trip time, τ_{RT}, can be expressed[1] by

$$\tau_{RT} = \frac{4D}{gI_{sp}} + 4\sqrt{\frac{Dm_f}{F}} \tag{1}$$

3

where D is the one way distance between the travel points, g the earth's gravitational acceleration, m_f the dry mass of the vehicle, F the thrust. The inverse dependence of
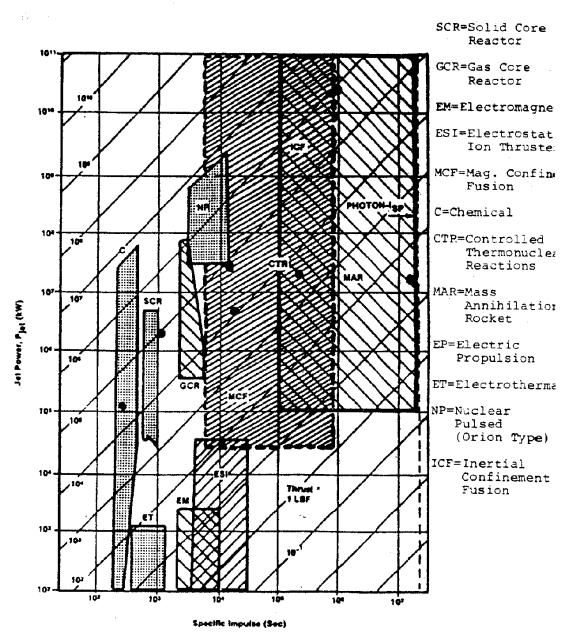

Fig. 1: Specific Impulse vs. Jet Power for Different Propulsion Systems

travel time on I_{sp} and F reveals dramatically the desirability of having both of these parameters as large as possible and feasible. Fig. 1 shows that present day chemical propulsion is capable of producing large thrusts but at a modest I_{sp} of about 450 seconds. Moreover, a great deal of propellant is required to lift the propellant itself up thereby

limiting the amount of payload that can be transported into space. Solid core fission rockets are capable of $I_{sp} \sim 1000$ seconds only due to the temperature limitations of its solid fuel elements. They are, however, capable of generating large thrusts, but they also must carry a great deal of propellant to compensate for the modest I_{sp}. The gas core fission rocket avoids the temperature limitations of SCR by using the fissionable fuel in a gaseous and indeed ionized form. It has been theoretically predicted[2], however, that such systems are capable of producing I_{sp}'s of about 2000 – 3000 seconds but major physics and engineering problems stand in the way of achieving these propulsive capabilities. It is also evident from Fig. 1 that next to the antimatter annihilation systems, fusion (CTR) occupies the largest domain in the propulsion parameter space of I_{sp} and jet power (including thrust), and as we shall see, the MICF system falls well within the shaded region identified as ICF or inertial confinement fusion.

2.0   Advanced Concept Description

2.1   Major Attributes of MICF

The effectiveness of MICF as a propulsion system resides with its ability to generate large energy magnification through fusion reactions that translate into very large particle escape velocities and correspondingly large specific impulses. This appears to be quite achievable in MICF pellets due to the presence of a large self-generated magnetic field that serves to thermally insulate the plasma from the metal shell that physically contains it. When a laser or a particle beam enters the target through a small hole, as depicted in Fig. 2, it ablates the fuel-coated inner wall not only at the spot of incidence but throughout the region as a result of photon scattering during the illumination process. If high enough energy is delivered by the incident beam, a hot plasma is created in the core which can immediately begin to undergo fusion reactions and produce energy. At the time of beam incidence, a shock wave is also set up at the inner face of the metal shell that begins instantly to traverse that medium outward. Its velocity is dictated by the density and the temperature of the shell, and the time it takes this sound wave to reach the outer surface constitutes the confinement time of the plasma within. This is estimated to be about 100 nanoseconds which is two orders of magnitude larger than that of implosion-type inertial fusion systems. Because of this long confinement time, more fusion reactions take place that result in greater magnification of the incident energy and a hotter plasma at the end of the burn. End of the burn is reached when the shock wave reaches the outer surface of the metal shell at which time the physical integrity of the pellet is no longer preserved and disassembly takes place. As the analysis below will show, energy gains ranging from several hundreds to a few thousands are achievable depending on pellet design and incident energy. This gain ultimately manifests itself in very energetic particles that emerge through the magnetic nozzle of a reaction chamber delivering $\sim 10^6$ seconds of specific impulse.

2.2   Detailed Technical Analysis

A mathematical formulation of the plasma dynamics in MICF follows the time evolution of the following sequence of events. Initially, the target pellet will consist of a
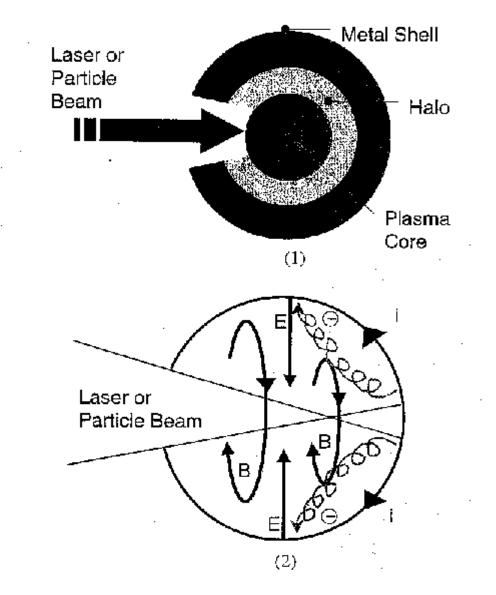

Fig. 2: Schematic of (1) Plasma Formation and (2) Magnetic Field Formation in MICF

metallic outer shell of outer radius r_{max}, coated internally by a layer of solid fuel with a central cavity of radius r_0. An incident beam ablates a portion of the fuel layer to form the core plasma and probably leaves the remainder of the fuel layer in a vaporized, partially ionized state. This partially ionized fuel layer we call the "halo". The outer radius of the halo is designated by r_1. Fig. 2(1) shows the three regions at a time when the beam is illuminating the interior.

By writing down a set of quasi one-dimensional time dependent balance equations for the constituents of a deuterium-tritium (DT) plasma and an appropriate number of fast alpha energy groups, we assess the reactor aspect of MICF by calculating the energy gain factor Q and identifying the relevant parameters that could lead to its enhancement. We allow for classical and anomalous diffusion across the magnetic field for the hot core plasma and the cooler plasma in the halo region and find that Q-values in the hundreds to thousands are achievable if certain assumptions are made regarding initial plasma parameters and refueling rates.

We assume that the hole through which the beam enters the pellet interior is small enough so that the resulting plasma is effectively spherically symmetric. The incident beam may not deposit all of its energy at the point where it strikes the interior wall; some of it may be reflected, but since the entry hole is small, it will remain within the cavity and eventually be absorbed elsewhere on the wall. Thus, we therefore assume that the wall temperatures are also spherically symmetric. Certainly, this symmetry should be reasonable once the beam is turned off and the fusion plasma becomes the sole source of energy for the system. It will also be assumed that the plasma is nearly uniform in the radial direction, with a sharp boundary where it meets the halo; the magnetic field is assumed to be trapped in a narrow gap between those two regions. We again assume that the halo is uniform in density, temperature, and (partial) ionization fraction. We treat the metal shell as having three regions, each of which is inertially uniform: the innermost of these is considered to be partially ionized; the second, which is bounded on its outer edge by the propagating shock wave, is treated as un-ionized but with a density and temperature which may vary with time; the third, outermost region is outside the shock wave and is assumed to be unaffected by the events within.

2.3   Basic Equations and Analysis

We treat the core plasma region as having three thermalized species: fuel ions, electrons, and alpha particles, plus an arbitrary number of fast alpha energy groups. The fuel ions have mass m_f, density n_f, and temperature T_f. Similarly, the electrons have mass m_e, density n_e, and temperature T_e, while the thermal alphas have mass m_α, density n_α, and temperature T_α. There are k_{max} fast alpha groups (also with mass m_α). For each group $1 \leq k \leq k_{max}$, the density is n_k and the energy is E_k. The various energies E_k are preset constants which do not vary with time; changes in the fast alpha energy distribution are accomplished by varying the densities n_k.

2.3.1   Fuel Ions

$$\frac{d}{dt}\left\{\frac{4}{3}\pi r^3 n_f\right\} = -\frac{4}{3}\pi r^3\left\{\frac{1}{2}n_f^2\langle\sigma v\rangle_f\right\} + 4\pi r^2\left\{\Gamma_r - \Gamma_f\right\} \tag{2}$$

$$\frac{d}{dt}\left\{\frac{4}{3}\frac{\pi r^3}{\gamma-1}n_f T_f\right\}+4\pi r^2 n_f T_f\frac{dr}{dt}=$$

$$\frac{4}{3}\pi r^3\left\{\frac{3}{2}\frac{n_f n_e}{(n\tau)_{ef}}(T_e-T_f)+\frac{3}{2}\frac{n_f n_\alpha}{(n\tau)_{\alpha f}}(T_\alpha-T_f)+n_f\sum_{k=1}^{k_{max}}n_k\left(\frac{dE_k}{dt}\right)_f-\frac{3}{4}n_f^2\langle\sigma v\rangle_f T_f\right\}+ \quad (3)$$

$$4\pi r^2\left(W_r-W_f\right)$$

In these equations, r is the radius of the plasma core, $\langle\sigma v\rangle_f$ is the velocity-averaged fusion reaction cross section, Γ_f and W_f the particle and energy fluxes respectively for fuel ions escaping from the plasma core, and Γ_r and W_r the particle and energy fluxes for the refueling fuel ions which cross the magnetic field region to enter the plasma core. The quantity $(n\tau)_{ef}$ is the energy exchange time constant for the electron-ion interaction while $(n\tau)_{\alpha f}$ is the corresponding one for the interaction between thermal alphas and fuel ions. The rate at which the k-th fast alpha group loses energy to the fuel ions is given by $\left(\frac{dE_k}{dt}\right)_f$, and γ is the adiabatic constant whose value is taken to be $\frac{5}{3}$.

2.3.2 Electrons

$$n_e = n_f + 2(n_\alpha + n_{f\alpha}) \quad (4)$$

$$\frac{d}{dt}\left\{\frac{4}{3}\frac{\pi r^3}{\gamma-1}n_e T_e\right\}+4\pi r^2 n_e T_e\frac{dr}{dt}=$$

$$\frac{4}{3}\pi r^3\left\{\frac{3}{2}\frac{n_e n_f}{(n\tau)_{ef}}(T_f-T_e)+\frac{3}{2}\frac{n_e n_\alpha}{(n\tau)_{\alpha e}}(T_\alpha-T_e)+n_e\sum_{k=1}^{k_{max}}n_k\left(\frac{dE_k}{dt}\right)_e-P_{BC}\right\}+ \quad (5)$$

$$4\pi r^2\left\{\Gamma_r E_{re}-(\Gamma_f+2\Gamma_\alpha)E_{le}\right\}$$

In Eqs. (4) and (5), Γ_α is the particle flux for alpha particles escaping from the plasma core. E_{re} is the average energy of an electron which diffuses across the magnetic field into the plasma core, while E_{le} is the average energy of an electron which diffuses out of the core. $(n\tau)_{\alpha e}$ is the energy exchange time constant for electrons interacting with thermal alphas and $\left(\frac{dE_k}{dt}\right)_e$ the rate at which the k-th fast alpha group loses energy to the electrons. P_{BC} is the bremsstrahlung radiation per unit volume from the core plasma electrons. Here we set E_{re} and E_{le} equal to the appropriate average electron energies, i.e.,

$$E_{re}=\frac{3}{2}T_l \quad ; \quad E_{le}=\frac{3}{2}T_e$$

2.3.3 Thermal Alphas

$$\frac{d}{dt}\left\{\frac{4}{3}\pi r^3 n_\alpha\right\} = \frac{4}{3}\pi r^3 L_{max} - 4\pi r^2 \Gamma_\alpha \tag{6}$$

$$\frac{d}{dt}\left\{\frac{4}{3}\frac{\pi r^3}{\gamma-1}n_\alpha T_\alpha\right\} + 4\pi r^2 n_\alpha T_\alpha \frac{dr}{dt} =$$

$$\frac{4}{3}\pi r^3\left\{\frac{3}{2}\frac{n_\alpha n_f}{(n\tau)_{\alpha f}}(T_f - T_\alpha) + \frac{3}{2}\frac{n_\alpha n_e}{(n\tau)_{\alpha e}}(T_e - T_\alpha) + n_\alpha \sum_{k=1}^{k_{max}} n_k \left(\frac{dE_k}{dt}\right)_\alpha + \frac{3}{2}L_{max}T_\alpha\right\} - \tag{7}$$

$$4\pi r^2 W_\alpha$$

In these last equations, W_α is the energy flux for thermal alphas diffusing out of the core, and $\left(\dfrac{dE_k}{dt}\right)_\alpha$ gives the rate at which the k-th fast alpha group gives up energy to the thermal alphas. L_{max} is the rate at which alpha particles slow down out of the lowest of the fast alpha energy groups and thus become part of the thermal alpha population. The lower energy bound of this group is set to $\dfrac{3}{2}T_\alpha$, and those alphas that cool down below this energy are assumed to be thermalized.

2.3.4 Fast Alphas

$$\frac{d}{dt}\left\{\frac{4}{3}\pi r^3 n_\alpha\right\} = \frac{4}{3}\pi r^3\left\{S_k - L_k\right\} \tag{8}$$

$$\frac{d}{dt}\left\{\frac{4}{3}\frac{\pi r^3}{\gamma-1}n_k \overline{E}_k\right\} + 4\pi r^2 n_k \overline{E}_k \frac{dr}{dt} =$$

$$\frac{4}{3}\pi r^3 \frac{3}{2}\left\{S_k E_{k-1} - L_k E_k - n_k\left[n_f\left(\frac{dE_k}{dt}\right)_f + n_e\left(\frac{dE_k}{dt}\right)_e + n_\alpha\left(\frac{dE_k}{dt}\right)\right]\right\} \tag{9}$$

Here, S_k is the rate at which alpha particles enter the k-th group, and L_k is the rate at which they leave it. We explicitly assume that fast alphas slow down much more rapidly than they diffuse out of the core, so that cross-field losses can be ignored during the slowing down process. For the first group (highest energy), S_1 is the rate at which high energy (3.5 MeV) alphas are produced by fusion, i.e.,

$$S_1 = \frac{1}{4}n_f^2 \langle\sigma v\rangle_f \tag{10}$$

The upper boundary of the k-th group is E_{k-1}, and the lower boundary is E_k. We therefore assume that

$$\overline{E}_k = \frac{1}{2}[E_{k-1} + E_k] \qquad (11)$$

Since alphas slowing down out of one group constitute the source for the next group, then

$$S_k = L_{k-1}, \qquad 2 \le k \le k_{max} \qquad (12)$$

Thus, if we solve the fast alpha equations in order from $k = 1$ to $k = k_{max}$, each pair of Eqs. (8) and (9) has two unknowns, n_k and L_k. Typically, we choose k_{max} to be 10 originally.

2.3.5 Halo Region

The fuel ions and associated electrons which lie outside the central core, between r and r_1, constitute the halo. This region can exchange ions (and energy) with the core region by cross-field diffusion. We assume, however (with perhaps some risk), that there is no exchange of ions or energy with the metallic shell which lies outside the halo region. Thus, our halo equations can be written as

$$\frac{d}{dt}\left\{ \frac{4}{3}\pi(r_1^3 - r^3)N_1 \right\} = -4\pi r^2[\Gamma_r - \Gamma_f] \qquad (13)$$

$$\frac{d}{dt}\left\{ \frac{4\pi(r_1^3 - r^3)}{3(\gamma-1)} N_1(1 + Z_{1E})T_1 \right\} + 4\pi\left[r_1^2 \frac{dr_1}{dt} - r^2 \frac{dr}{dt} \right] N_1(1 + Z_{1E})T_1 =$$

$$4\pi\{ r^2\phi(r) - r_1^2\phi(r_1) \} - \frac{4\pi}{3}(r_1^3 - r^3)\frac{d}{dt}(N_1 E_{Z1}) + \qquad (14)$$

$$4\pi r^2\{ W_f + W_\alpha - W_r + (\Gamma_f + 2\Gamma_\alpha)E_{Le} - \Gamma_r E_{re} \}$$

where N_1 is the density of fuel ions plus atoms in the halo region. We assume that this region contains only un-ionized fuel atoms, fuel ions, and electrons. Since the atoms in this region are only partially ionized, they have an effective charge Z_{1E} which depends on the temperature T_1. The quantity E_{Z1} represents a "latent heat" of ionization. The terms $\phi(r)$ and $\phi(r_1)$ are the bremsstrahlung fluxes per unit area across r and r_1 respectively. Thus, the first term on the right hand side of the above equation represents the radiative heating of the halo region.

2.3.6 Metallic Shell

We break up the metallic shell into three regions. The innermost from r_1 to r_2 is considered to be partially ionized, with an effective charge number Z_{2E}. This region has a density (ions plus un-ionized atoms) N_2 and a temperature T_2. For this region, the density and energy equations are

$$\frac{d}{dt}\left\{\frac{4}{3}\pi\left(r_2^3 - r_1^3\right)N_2\right\} = 0 \tag{15}$$

$$\frac{d}{dt}\left\{\frac{4\pi\left(r_2^3 - r_1^3\right)}{3(\gamma-1)}N_2(1+Z_{2E})T_2\right\} + 4\pi\left[r_2^2\frac{dr_2}{dt} - r_1^2\frac{dr_1}{dt}\right]N_2(1+Z_{2E})T_2 =$$

$$4\pi\left\{r_1^2\phi(r_1) - r_2^2\phi(r_2)\right\} - \frac{4\pi}{3}\left(r_2^3 - r_1^3\right)\frac{d}{dt}(N_2 E_{Z2}) \tag{16}$$

where E_{Z2} represents the "latent heat" of ionization for the material and the first term on the right hand side represents the bremsstrahlung heating of this region. Actually, we would expect a continuous variation of Z_{2E} and T_2 with radius, with Z_{2E} becoming zero for sufficiently large radii. For ease of calculation, however, we assume the temperature to be constant over this region, and that the following region also has a constant temperature, but no ionization. The un-ionized metallic shell region extends from r_2 to r_3 and has a density N_3 and temperature T_3. To keep the calculation manageable, we have assumed that there is no flux of particles or energy across either of these borders. For the un-ionized region, the density and energy equations are

$$\frac{d}{dt}\left\{\frac{4}{3}\pi\left(r_3^3 - r_2^3\right)N_3\right\} = 4\pi r_3^2 N_{sol}\frac{dr_3}{dt} \tag{17}$$

$$\frac{d}{dt}\left\{\frac{4\pi\left(r_3^3 - r_2^3\right)}{3(\gamma-1)}N_3 T_3\right\} + 4\pi\left[r_3^2\frac{dr_3}{dt} - r_2^2\frac{dr_2}{dt}\right]N_3 T_3 =$$

$$4\pi\left\{r_2^2\phi(r_2) - r_3^2\phi(r_3)\right\} + 4\pi r_3^2\left\{\frac{3}{2}N_{sol}T_3\frac{dr_3}{dt}\right\} \tag{18}$$

The outer radius, r_3, of this region is fixed at the shock wave, which moves with the local speed of sound outward through the shell. Thus, while we assume no movement of matter or energy (except for bremsstrahlung radiation) across the boundary at r_2, the outward movement of the shock wave is constantly incorporating more material into the un-ionized shell region. The portion of the metallic shell outside r_3 constitutes a third shell region; however we do not provide any balance equations for this region. Its only effect on the inner regions comes through the temperature of the matter incorporated into the 3 region via the motion of r_3. We assume that the density of this outer region is the unperturbed solid N_{sol}, and that the temperature of the matter incorporated by the motion of r_3 is just T_3 which is the temperature of the un-ionized region inside r_3. This latter assumption may not be fully justified since the region below r_3 is subject to adiabatic compression heating as well as bremsstrahlung, while the region outside r_3 is affected by bremsstrahlung only.

2.3.7 Bremsshrahlung Radiation

As we have indicated in the equations above, the bremsstrahlung emitted by the hot core electrons may cause an appreciable ablation of the inner wall of the shell which initially is composed of DT fuel in the solid state. The rate at which bremsstrahlung carries energy out of the core is $\frac{4}{3}\pi r^3 P_{BC}$ where the radiated power per unit volume is

$$P_{BC} = \left(3.340\times10^{-15}\right)n_e T_e^{\frac{1}{2}}\left[n_f + 4\left(n_\alpha + \sum_{k=1}^{k_{max}} n_k\right)\right] \quad \frac{keV}{cm^3 \cdot s} \tag{19}$$

In a planar geometry of a monoenergetic beam of photons, the energy flux can be expressed by

$$\phi(x) = h\int_0^\infty \nu I_\nu(x)dx \tag{20}$$

where $h\nu$ is the energy per photon and I_ν the beam intensity. The absorption coefficient K_ν is given by[3]

$$K_\nu = \frac{4}{3}\left(\frac{2\pi}{3T}\right)^{\frac{1}{2}}\frac{N^2 Z^3 e^6}{hcm_e^{\frac{3}{2}}\nu} \tag{21}$$

where N is the ion density, T the electron temperature, and Z the ionic charge in the absorbing medium. The electron mass is denoted by m_e, its charge by e, and the speed of light by c. Using the following values

$$h = 4.135\times10^{-18} \quad keV\cdot s$$
$$e^2 = 1.44\times10^{-10} \quad cm\cdot keV$$
$$m_e = \frac{1}{1836.1} \; amu = \frac{1.043937\times10^{-15}}{1836.1} \quad keV\cdot s^2 \cdot cm^2$$
$$c = 2.99793\times10^{10} \quad cm\cdot s^{-1}$$

we obtain

$$K_\nu = \left(7.6651\times10^{-48}\right)\frac{Z^3 N^2}{T^{\frac{1}{2}}(h\nu)^3} \quad cm^{-1} \tag{22}$$

when N is given in cm^{-3} and both T and $h\nu$ are expressed in keV.

If the incident bremsstrahlung is emitted by a plasma whose electrons have a Maxwellian velocity distribution characterized by the temperature T_o, then the emitted energy density J_ν is given by[4]

$$J_v dv = \frac{32\pi}{3} \left(\frac{2\pi}{3m_e T_o} \right)^{1/2} \frac{Z_o e^6 N_+ N_-}{m_e c^3} \exp\left(-\frac{h\nu}{T_o} \right) dv \tag{23}$$

where N_+ is the density of the ions, Z_o the ionic charge, and N_- the electron density in the emitting plasma. Setting $N_+ = N_o$ and $N_- = Z_o N_o$, this becomes

$$J_v = \left(1.253614 \times 10^{-32} \right) \frac{Z_o^3 N_o^2}{T_o^{1/2}} \exp\left(-\frac{h\nu}{T_o} \right) \tag{24}$$

where N_o is in cm^{-3} and T_o and $h\nu$ are in keV. If the plasma volume is V_o and the surface area A_o since J_v is an energy density,

$$\phi(x) = \frac{V_o}{A_o} \int_0^\infty J_v \exp(-K_v x) dv \tag{25}$$

The above equation has been derived for plane geometry; however, switching to spherical geometry introduces very little change. The spherical analogue is given by

$$\phi(r) = \frac{r_o^3}{3r^2} \int_0^\infty J_v \exp[-K_v (r - r_1)] dv \tag{26}$$

If there is an absorber shell of thickness Δ_1 in the region between r_o and r_1, characterized by an absorption coefficient K_{1v}, and an absorber between r_1 and r characterized by K_{2v}, then one can show after some manipulation that we can write

$$\phi(r) = C_o P(\alpha) \tag{27}$$

where

$$P(\alpha) = \int_0^\infty \exp\left[-\left(W + \frac{\alpha^3}{W^3} \right) \right] dW \tag{28}$$

and

$$C_0 = \left(1.0106 \times 10^{-15} \right) Z_o^3 N_o^2 T_0^{1/2} \frac{r_o^3}{r^2} \tag{29}$$

13

$$\alpha = \frac{\left(1.9717 \times 10^{-16}\right)}{T_o} \left[\frac{Z_1^3 N_1^2}{T_1^{1/2}} \Delta_1 + \frac{Z_2^3 N_2^2}{T_2^{1/2}} (r - r_1) \right]^{1/3} \tag{30}$$

We have found that we can approximate the integral $P(\alpha)$ in (28) by the algebraic form

$$P(\alpha) \cong \frac{1}{D} e^{-(0.43)\alpha} \tag{31}$$

where

$$D \equiv 1.000 + (0.924)\alpha + (0.040)\alpha^2 + (0.065)\alpha^3 \tag{32}$$

This form is quite accurate for small α. For large α, the relative error may be large, but $P(\alpha)$ becomes so small that the absolute error is negligible for our purposes.

2.3.8   Partial Ionization

The degree of ionization in a material at thermal equilibrium depends on the temperature of the material. The Saha equation represents a commonly used approach to describing how the ionization state varies with temperature. We have approximated the standard form of this equation[5] by ones that apply directly to the regions of interest in MICF. For example, when applied to the fuel ions with a single charge only, in the halo region we let

$$Z_{1E} = 1.0 - \exp(-y) \tag{33}$$

where

$$y = \frac{x\left[1.0 + (0.05)x^2\right]}{1.0 + (1.3)x^{9/4}} \tag{34}$$

and

$$x = \frac{1.382 \times 10^{13} T_1^{3/4}}{n_1^{1/2}} \exp\left(-\frac{0.0068}{T_1}\right) \tag{35}$$

Once Z_1 has been calculated, the energy required to achieve that degree of ionization is just

$$E_{Z1} = \left(1.36 \times 10^{-2}\right) Z_1 \tag{36}$$

14

Similar formulas were deduced for tungsten whose $Z_2 = 74$. If we define the energy E_{Z0} required to completely ionize a tungsten atom as

$$E_{Z0} = 277.387 \qquad keV$$

then the energy needed to achieve the ionization state Z_{2E} is

$$E_{Z2} = E_{Z0}\left[1.0 - \exp\left(\frac{y_1}{E_{Z0}}\right)\right] \tag{37}$$

where the parameter y_1 is given by

$$y_1 = yI_1\left[1.0 + \frac{(I_1 x)^{5/4}\left(1.8\times10^{-6}\right)n_2^{0.35}}{1.0 + (I_1 x)^{1/2}}\right] \tag{38}$$

In this equation, y is a constant expressed in terms of the density and the temperature of the region, and $I_1 = 7.98\times10^{-3}$ keV is the energy needed to strip away the first electron from a tungsten atom, i.e., the energy required to form a singly-ionized tungsten ion. The above formulas can be applied to other heavy metals such as gold, often considered for MICF targets but not necessarily with the same numerical factors.

2.3.9 Additional Relevant Formulas

Before any meaningful results can be obtained from the preceding equations, several formulas must be supplied for a number of the quantities that appeared therein. In some cases, just the general formula will be listed keeping in mind that numerical values will depend on the species involved including mass, charge, density, and temperature.

A.   Fusion Cross Section

An excellent fit to the measured velocity averaged fusion cross section for DT is given by[6]

$$\langle\sigma v\rangle_f = \frac{\left(3.05\times10^{-13}\right)\exp\left[-\dfrac{17.7}{T_f^{0.348}}\right]}{1.0 + 0.1554T_f^{1/3} - 0.1418T_f^{2/3} - 0.05T_f + 0.0364T_f^{4/3}} \tag{39}$$

This formula gives results which agree with the numerically tabulated values of Greene[7] to within 2.7% for fuel temperatures between 1.0 and 500 keV.

B. Energy Exchange Between Maxwellian Species

The time constant $(n\tau)_{ij}$ for energy exchange between species i and j can be expressed by the general formula[8]

$$(n\tau)_{ij} = \frac{\sqrt{\frac{2}{\pi}}}{8Z_i^2 Z_j^2 e^4} \frac{m_j}{m_i^{1/2}} \left(T_i + \frac{m_i}{m_j} \right)^{3/2} \frac{1}{\ln\lambda_{ij}} \tag{40}$$

which in the case of alpha-fuel ion interaction, for example, assumes the form

$$(n\tau)_{\alpha f} = \left(3.88510\times10^{10}\right) \frac{m_j}{m_i^{1/2} \ln\lambda_{\alpha f}} \left(T_\alpha + \frac{m_\alpha}{m_f} \right)^{3/2} \tag{41}$$

where the Coulomb logarithm term contains[9]

$$\lambda_{\alpha f} = \left(8.680555\times10^{14}\right) \left(\frac{T_\alpha T_f T_e}{n_e} \right)^{1/2} \tag{42}$$

C. Fast Alpha Slowing Down

The energy loss per unit time when a fast alpha slows down in an ion (including thermal alphas) whose thermal velocity is much smaller than the velocity of the incident alpha can be written as[8]

$$\left(\frac{dE_\alpha}{dt} \right)_j = -\frac{4\pi}{\sqrt{2}} Z_\alpha^2 Z_j^2 e^4 \frac{n_j}{m_j} \frac{m_\alpha^{1/2}}{E_\alpha^{1/2}} \ln\lambda_j \tag{43}$$

while for fast alpha slowing down on electrons whose thermal velocity is still generally greater than the fast alpha velocity the result is

$$\left(\frac{dE_\alpha}{dt} \right)_e = -\frac{16}{3} \sqrt{\frac{\pi}{2}} Z_\alpha^2 e^4 \frac{n_e m_e^{1/2}}{m_\alpha} \frac{E_\alpha}{T_e^{3/2}} \ln\lambda_e \tag{44}$$

where

$$\lambda_e = \left(3.307054\times10^{14}\right) \frac{T_e}{n_e^{1/2}} \tag{45}$$

16

Similar formulas can be written with the appropriate constants from Eq. (43) for the interactions with the fuel ions and thermal alphas.

D.   Pressure Gradients

We readily obtain the pressure gradient within a given region as ΣnT summed over the species (including electrons) present in the region. However, since a pressure is assumed to apply everywhere within its region, we would obtain infinite pressure gradients at the boundaries between regions. To get around this problem, we assume a form for the pressure dependence upon radius, which can then be fitted to the pressures in tow adjacent regions to provide the pressure and pressure gradient at the boundary. Since the pressure in adjacent regions often differ by several orders of magnitude, we choose a logarithmic relationship

$$\ln P = \left(\frac{r_1 + b - r}{2b}\right)\ln P_1 + \left(\frac{r - r_1 + b}{2b}\right)\ln P_2 \qquad (46)$$

where the first region extends from r_o to r_1, the second region goes from r_1 to r_2, and the parameter b is the "inverse average" of the thickness of the two regions, i.e.,

$$\frac{1}{b} = \frac{1}{2}\left[\frac{1}{r_1 - r_o} + \frac{1}{r_2 - r_1}\right] \qquad (47)$$

Setting $r = r_1$ in Eq. (46) it yields

$$P = \sqrt{P_1 P_2} \qquad (48)$$

$$\frac{\partial P}{\partial r} = \frac{P}{2b}\ln\left(\frac{P_2}{P_1}\right) \qquad (49)$$

This pressure gradient is used in the calculation of the diffusion across the magnetic field, and also in the calculation of the various shell boundaries.

E.   Diffusion Across the Magnetic Field

It seems likely that diffusion across the magnetic field will obey the classical diffusion law for which the following formulas have been obtained and adapted to the MICF scheme[10]. A Bohm diffusion term[11] has also been included for completeness so that we can write using subscript "C" to denote classical and subscript "B" to denote Bohm:

$$\Gamma = \left(1 - C_{Bohm}\right)\Gamma_C + C_{Bohm}\Gamma_B \qquad (50)$$

$$W = (1 - C_{Bohm})W_C + C_{Bohm}W_B \tag{51}$$

where Γ_C and W_C are the classical fluxes and Γ_B and W_B the Bohm fluxes and C_{Bohm} an arbitrary constant. The classical diffusion coefficient includes the product of the "step size" in a random walk across the field and a collision frequency. The step size is the Larmor radius while the collision frequency should include collisions with all the species in the region. The Bohm diffusion is identified with plasma turbulence instability associated with density and/or temperature gradients and its coefficient has the form

$$D_B = \frac{T}{16eB} = (6.25 \times 10^5)\frac{T}{B} \tag{52}$$

where e is the electronic charge, and B the strength of the magnetic field. Noting that for charge neutrality,

$$\Gamma_e = \Gamma_f + 2\Gamma_\alpha \tag{53}$$

the particle and energy fluxes via Bohm diffusion can be written as

$$(\Gamma_f)_B = (6.25 \times 10^5)\frac{T_e}{B}\left(\frac{\partial n_f}{\partial r}\right) \tag{54}$$

$$(\Gamma_\alpha)_B = (6.25 \times 10^5)\frac{T_e}{B}\left(\frac{\partial n_\alpha}{\partial r}\right) \tag{55}$$

$$(W_f)_B = (9.375 \times 10^5)\frac{T_f T_e}{B}\left(\frac{\partial n_f}{\partial r}\right) \tag{56}$$

$$(W_\alpha)_B = (9.375 \times 10^5)\frac{T_\alpha T_e}{B}\left(\frac{\partial n_\alpha}{\partial r}\right) \tag{57}$$

For the classical diffusion of fuel ions across the magnetic field into the core plasma, we use the basic diffusion formula keeping in mind that collisions in this region are only with the electrons since no alphas are created there or

$$(\Gamma_r)_C = \frac{8\sqrt{\pi}}{3}\left(\frac{e}{b}\right)^2 \frac{\left(\frac{m_e}{2\Gamma_e}\right)^{1/2}\ln\lambda_{er}}{\left(1 + \frac{m_e T_r}{m_f T_e}\right)^{3/2}}\left\{\left(1 + \frac{m_e}{m_f}\left(\frac{T_r}{T_e} - 1\right)\right)n_r\frac{\partial n_e}{\partial r} - \left(1 + \frac{m_e T_r}{m_f T_e}\right)\frac{\partial}{\partial r}(n_r n_e)\right\} \tag{58}$$

18

In this equation, the quantities n_e and T_e do not have the same meaning as in the other equations cited so far. T_e is this case refers to the temperature of the electrons in the halo region between r_1 and r which is not equal to the temperature of the core plasma electrons. The electron density n_e should be equal to n_r, the density of the fuel ions in the halo region rather than the density of the core plasma electrons. For the density gradient in the halo region, we use

$$\frac{\partial n}{\partial r} = \left(\frac{r}{r_1 - r}\right)\left(\frac{\partial P}{\partial r}\right) \tag{59}$$

where $\dfrac{\partial P}{\partial r}$ is calculated from Eq. (49).

2.3.10 Expansion Rates

The advantage of Magnetically Insulated Inertial Confinement Fusion is that the expansion of the plasma core is inhibited by the presence of a solid outer shell. As the plasma attempts to expand, it pushes on the halo, which is compressed and in turn pushes on the metallic shell. The various metallic shell regions are similarly compressed and exert pressure on the regions outside themselves. Thus a pressure (shock) wave is set up which propagates outward at the local speed of sound. The speed of this shock wave, assuming there is negligible back pressure outside the shock wave is given by

$$u_3 = \frac{dr_3}{dt} = \sqrt{\frac{P_3}{\rho_3}} = \left[\frac{N_3 T_3}{\left(1.043937 \times 10^{-15}\right)\left(m_s + Z_2 m_e\right)N_{sol}}\right]^{\frac{1}{2}} \tag{60}$$

where m_s is the mass of a metal ion in the shell. The shock speed is a function of the local temperature; we like this temperature to be that of the preceding metallic shell region since we have no other evaluation of the temperature in the boundary zone. Once the shock wave reaches the outer limit (r_{max}) of the metallic shell, we assume that the physical integrity is lost so that further expansion is purely inertial and the fusion reaction is rapidly quenched. Hence the calculations cease when $r_3 = r_{max}$.

The expansion speed of each of the inner boundaries is found from a momentum balance equation of the form

$$mN\frac{du}{dt} = -\frac{1}{r^2}\frac{d}{dr}\left(r^2 P\right) \tag{61}$$

The pressure gradients are obtained using Eqs. (49) and (57). The mass m and density N should be those of the boundary region. Since these are undefined, we take the quantity mN to be the average mass times density products in the two adjacent regions. We therefore have

$$\frac{du}{dt} = \frac{d}{dt}\left(\frac{dr}{dt}\right) = \frac{-2\left[2\dfrac{P(r)}{r} + \dfrac{\partial P(r)}{\partial r}\right]}{\left(1.043937\times10^{-15}\right)\left[m_f N_f + m_e N_e + m_\alpha \left(N_\alpha + N_{f\alpha}\right) + \left(m_f + m_e\right)N_1\right]} \tag{62}$$

with explicit expression for $\dfrac{du_1}{dt}$ and $\dfrac{du_2}{dt}$. If the gradient $\dfrac{\partial\left(r^2 P\right)}{\partial r}$ is positive, the velocity derivative $\dfrac{du}{dt}$ is negative. Should this condition hold for a sufficiently long time, it is possible for the speed to become negative. In our simulation, this does in fact occur and is critical for the generation of a significant amount of fusion power. Were it not for the requirement that

$$r < r_1 < r_2 < r_3 \tag{63}$$

combined with the limitation on $\dfrac{dr_3}{dt}$ given by Eq. (60), this compression of plasma would not occur and our gains Q would be quite modest. Since we are assuming no energy transport across the boundaries r_1 and r_2 except for the bremsstrahlung, this radiation may play an important role in slowing down the expansion of the core and increasing Q.

2.3.11 Alpha Source

We recall that the source term for the thermal alphas is L_{max}. The last (k_{max}) fast alpha group is treated somewhat differently from the others, so that some further discussion is warranted. Unlike the other fast alpha groups, the lower energy boundary for this group is not a preset number but instead is set equal to $\dfrac{3}{2}T_\alpha$. Thus,

$$\overline{E}_{k\,max} = \frac{1}{2}\left[E_{k\,max-1} + \frac{3}{2}T_\alpha\right] \tag{64}$$

Unlike the other groups, this average energy is not a constant, but has the derivative

$$\frac{d\overline{E}_{k\,max}}{dt} = \frac{3}{4}\frac{dT_\alpha}{dt} \tag{65}$$

This additional factor must be kept in mind in solving Eq. (9) for L_{kmax}.

In the course of a calculation, it may happen that T_α rises sufficiently to make $\dfrac{3}{2}T_\alpha \geq E_{k\,max-1}$. Since we would get into a serious computational difficulty if E_{kmax} were allowed to approach too close to $E_{k\,max-1}$, we must merge the k_{max} fast alpha group with

the (k_{max} – 1) group when the energy difference $\left(E_{k\,max-1} - E_{k\,max}\right)$ becomes small. This of course reduces k_{max} by one. We would not have this problem if we made k_{max-1} large enough that it always remains well above $\frac{3}{2}T_\alpha$, but such a procedure would reduce to some extent the accuracy of the solution.

2.3.12 Stability Considerations

Although no attempt was made to carry out an exhaustive study of the stability problem in MICF, we have identified the most likely modes and assessed their impact on the energy multiplication capability of the system. Numerical simulations[12] have shown that while the density increases outward from the center towards the halo region, the temperature drops over the same distance, allowing the pressure to remain nearly constant, i.e., $\nabla P = 0$. The plasma pressure remains constant also in the halo region, while the jump in its value occurs across the magnetic field that separates the two regions.

The stability of a high beta (ratio of plasma pressure to magnetic field pressure) plasma with gradients in density, temperature, and magnetic field has been examined by Aydemir, et al[13], who have shown that the two important parameters are

$$\tau = \frac{T_e}{T_i} \;\; ; \;\; \delta = \frac{\partial \ln B}{\partial \ln T_i} \tag{66}$$

With $\tau < 1 + \sqrt{2}$ as it is in MICF, the finite Larmor radius (FLR) modes are stable when $\delta < 0$, while the zero Larmor radius (ZLR) modes are stable when $\delta > \frac{0.5}{1+\tau}$. In MICF, the FLR modes are stable since $\delta \cong -1$, while the ZLR modes may not be stable. However, upon close examination, it appears that neither of these modes is likely to occur in MICF, or if they do, they constitute at best very weak instabilities. This is so because the magnetic field gradient in the region of interest is zero (i.e., $\delta = 0$) since the field variation follows that of the plasma pressure, and as we have already noted, $\nabla P = 0$.

This clearly leaves those modes that can arise in a high beta plasma with $\nabla P = 0$, situated in a constant magnetic field. This instability has been studied by Mikhailovski[14], and is characterized by the frequency

$$\omega = \frac{2}{3}\omega_r \left[1 \pm \frac{i}{\sqrt{2}}\right] \tag{67}$$

where ω_r is the drift frequency. Such an instability gives rise to ambipolar diffusion characterized by the coefficient

$$D = \frac{\gamma}{k_\perp^2} \;\; ; \;\; \gamma = \frac{\sqrt{2}}{3}\omega_r \tag{68}$$

21

where the perpendicular wave length $k_\perp^{-1}$ is set approximately equal to the plasma radius. We label such a diffusion as "modified Bohm" since we have already used the conventional Bohm diffusion to represent the anomalous transport in some of the cases we have examined. Conventional Bohm is generally associated with collisionless, magnetized plasma and its adaptability to MICF plasma may be questionable since the plasma in this case is likely to be highly collisional. Nevertheless, the use of conventional Bohm is perhaps justified to dramatize the impact of anomalous transport and associated turbulence on the performance of MICF. As we shall note shortly, the modified Bohm can result in Q-values exceeding a thousand, re-affirming the notion that such transport can lead to a more efficient fueling of the hot plasma without degrading its temperature.

3.0   Calculations Procedure and Results

3.1   Calculations Procedure

A large number of computational runs were made in order to produce a comprehensive parameter study of the MICF system for potential utilization in space propulsion. For each run, the initial density, temperature, and radius of the hot plasma core species are specified. While the initial temperatures of the core electrons and ions may each be specified separately, for most of these runs the two were set equal. The thermal alpha temperature was always set equal to that of the core fuel ions, while the densities of thermal alphas and fast alpha groups were set to achieve an appropriate equilibrium in the slowing down process. In addition, the initial density and temperature for the halo, "ionized" metallic shell, and "un-ionized" metallic shell regions were specified, as were the boundary radii. Judging by the trends displayed by the governing equations, it was not necessary to start the halo and metallic temperatures too low. The inner edge of each of these regions should become quite hot almost instantaneously. We, therefore, chose to set the initial halo temperature $T_1 = 0.10\,\text{keV}$ and the initial metallic shell temperatures $T_2 = T_3 = 0.01\,\text{keV}$ and these choices appeared to be reasonable.

The shock wave velocity u_3 is calculated while the other velocities are guessed at, but after a few iterations, these velocities settle down to their proper values. While the specified values for r_o, the initial cavity radius, and r_1, the initial other radius of the solid fuel, are design parameters, the value of r_2 of the boundary between the "ionized" and "un-ionized" metal is arbitrary, but its selection was guided once again by equations and known values of densities, etc. We set the shock wave position r_3 a small distance beyond r_2 initially, since it should be located in the non-ionized metal, but initially should be just outside the ionized region.

The time-dependent differential equations are then solved to obtain the various densities, temperatures, radii, and velocities for each time step until the calculation is halted. We end the calculation when the shock wave reaches r_{max}, the specified radius of the metallic shell. At this point, presumably the physical integrity of the metallic shell is lost; from then on the expansion of the plasma core becomes purely inertial so that the plasma rapidly dissipates and cools, quenching the fusion reaction. Since our equations do not have this loss of physical integrity built in, we use the arbitrary cut-off on plasma

radius in its place. For some runs, the shock wave never reaches r_{max}, since we also halt the computation if the plasma ion temperature in the core drops below $0.50\,keV$. Below this temperature, the fusion cross section $\langle \sigma v \rangle_f$ is so small that there seems little chance of enough fusion energy being generated to re-heat the plasma and the gain Q is no longer changing appreciably with time.

3.2 Results

It appears that for most parameter ranges, the gain Q is considerably larger if the diffusion is classical than if it is anomalous (Bohm). Fig. 3 shows a typical result; over much of the range Q is an order of magnitude larger for classical diffusion than for Bohm diffusion. However, while the anomalous diffusion exemplified by Bohm appears to give a lower gain than does the classical, the "modified Bohm" addressed in the section on stability appears to provide higher gain than classical. Fig. 4 shows the gains obtained for the same pellet and initial density as in Fig. 3. Note that the gains in Fig. 4 are about an order of magnitude higher than the classical diffusion of Fig. 3, and almost two orders higher than the Bohm results reaching a high value of Q = 2623 at E_{in} = 1.15 MJ. The high gain regime in Fig. 4 thus also extends downward farther than those of Fig. 3, which dropped rapidly below 2.6 MJ.
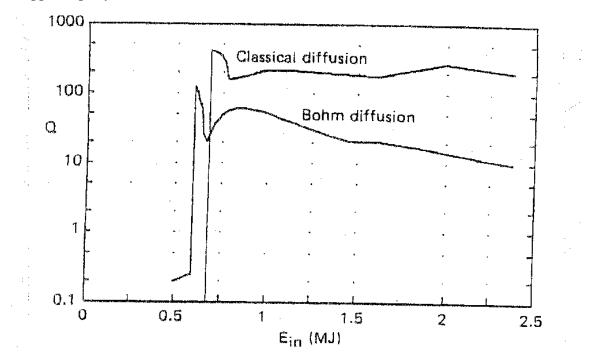

Fig. 3: Gain Q vs. Input Energy E_{in}. B = 100 T, N = 5×10^{21} cm^{-3}, r_o = 0.15 cm, r_f = 0.18 cm, r_{max} = 0.6 cm.
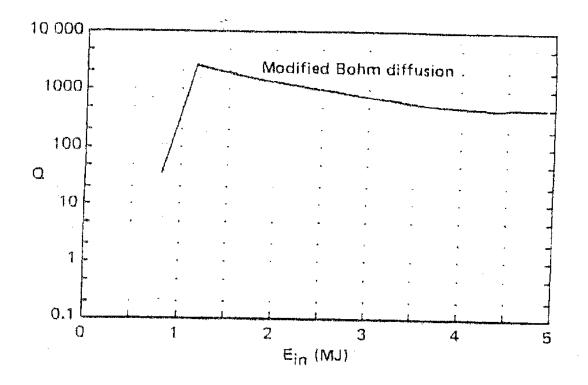
Fig. 4: Gain Q vs. Input Energy E_{in} for Modified Bohm Diffusion.
Initial $N = 5 \times 10^{21}$ cm^{-3}, $r_o = 0.15$ cm, $r_f = 0.18$ cm, $r_{max} = 0.6$ cm.

Fig. 3 also demonstrates the typical behavior of the results as the input energy E_{in} is varied. The gain generally increased as E_{in} decreased, although this behavior is not completely monotonic. However, there seems to exist a "cut-off" input energy below which Q becomes extremely small. This behavior is shown again in Fig. 5, which is for a smaller pellet (0.6 cm outer radius instead of 1.0 cm) but otherwise similar parameters. The maximum gains possible with this smaller pellet are somewhat lower in the case of classical diffusion, though roughly comparable in the case of Bohm diffusion, but away from the cut-off energy seem to be comparable in both cases. The major difference to be noted between Figs. 3 and 5 is the range of E_{in} in each. For the larger pellet (Fig. 3), the cut-off energy is about 2.5 MJ, while for the smaller pellet (Fig. 5), the cut-off energy occurs at 0.6 MJ for Bohm diffusion, and 0.7 for classical.
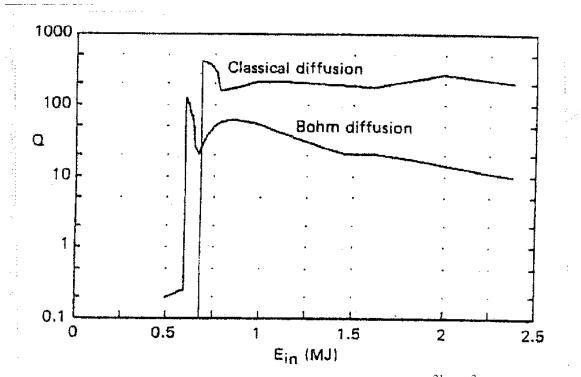
Fig. 5: Gain Q vs. Input Energy E_{in}. B = 100 T, N = 5×10^{21} cm^{-3}, r_o = 0.15 cm, r_f = 0.18 cm, r_{max} = 0.6 cm.

During a single run, the typical behavior is that the fuel ion temperature T_f initially drops while the density N_f increases. This latter effect is due to a more rapid diffusion into the core from the cool, dense halo then outward from the hot, diffuse core plasma. In those cases where the gain Q remains small, the temperature plunges so low that there is little fusion energy produced. If, however, the initial temperature and density were large enough, T_f goes through a minimum and begins to rise again. If this temperature can be maintained for a long enough period, an appreciable amount of fusion occurs and Q becomes quite large. Fig. 6 shows such a behavior; T_f rises to 227 keV and drops off very slowly beyond, falling to 74 keV at 100 ns when the shock wave reaches the wall. Most of the fusion energy was produced during the period when the pressure P was high; the gain at 24 ns was Q = 259, while the final gain (at 100 ns) was Q = 303. Thus, while we have specified an outer radius r_{max} for the shell of 1.0 cm, the gain would be almost as large if the radius was r_{max} = 0.4 cm, the shock wave radius at 24 ns.

The diffusion process plays a very important role in determining the temperature behavior. A net influx of fuel ions is helpful to the fusion process in that it builds up the density; since the fusion rate is proportional to the square of the density, this build-up can increase Q quite significantly. However, the incoming ions are much cooler than those of the central core, so that a high inward flux tends to cool the core. In the neighborhood of 5 keV and lower, the drop off in $\langle \sigma v \rangle_f$ with decreasing temperature becomes quite sharp, so that the increase in density may well be offset by the decrease in $\langle \sigma v \rangle_f$. The turnaround in fuel ion temperature shown in Fig. 6 occurred only after the halo had been
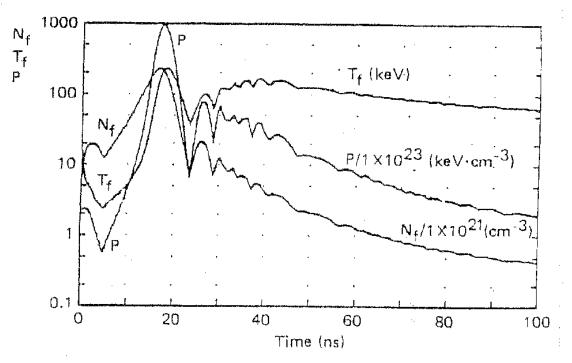
25

Fig. 6: Fuel Properties vs. Time for $E_{in} = 4.033$ MJ. B = 100 T, $r_o = 0.25$ cm, $N = 5 \times 10^{21}$ cm^{-3}, $T_o = 20$ keV

almost completely depleted (at 3.0 ns). In Fig. 7, we see that the radius r of the core increased for small times, while the outer radius r_1 of the halo remained virtually constant until $r_1 - r$ became very small. From that point onward, r_1 and r necessarily go in step since we consider the halo to be depleted and arbitrarily set

$$\frac{du_1}{dt} = \frac{r_1}{r}\frac{du}{dt}$$

Under our assumptions, at that point the fluxes into and out of the core become zero. While we might expect metallic shell ions to begin flowing into the core at that point their large charge number may serve to inhibit such incoming flux sufficiently for our assumption to be reasonably justified.

A typical behavior is seen in Fig. 7 where the plasma core contracts shortly after the depletion of the halo, reaching a minimum in this case near 18 ns, just about where the pressure maximum occurs. Meanwhile, r_2, the outer radius of the ionized metal, and r_3, the shock wave position, are increasing monotonically. The result is the Q plot as a function of time shown in Fig. 8. We observe that most of the gain occurs during the "compression" phase of the core plasma behavior.
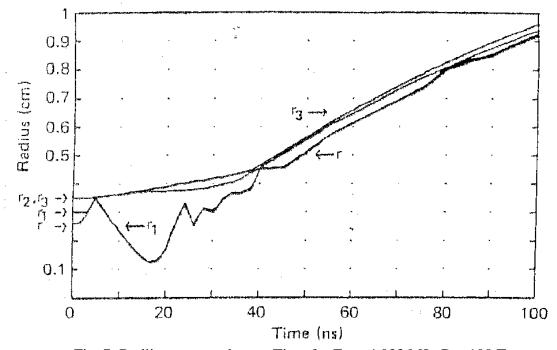
26

Fig. 7: Radii r, r_1, r_2, and r_3 vs. Time for E_{in} = 4.033 MJ. B = 100 T,
N = 5×10^{21} cm^{-3}, T_o = 20 keV, Classical Diffusion.

Since diffusion plays such an important role in determining the gain for an MICF reactor, it is not surprising that our assumption for the value of the magnetic field strongly affects the results. For most of our runs, we have used the value of 100 tesla. One set of runs done with various magnetic field values suggests that this may be near the optimum value. Fig. 9 shows Q falling off rather rapidly for small fields, and also falling, if less precipitously, as the field increases above 100 tesla.

The cut-off gain Q also scales with r_o up to almost r_o = 0.3 cm for classical diffusion; for Bohm diffusion, however, Q falls slightly as r_o increases. On the whole, since achieving the indicated input energies is likely to be one of the major challenges for MICF, it appears that the smaller the pellet, the better off we will be. The initial guess for the plasma density N_o appears to have relatively little effect on the results for densities in the range $1.5 \times 10^{21} \leq N_o \leq 5 \times 10^{21}$, although there are indications that still higher densities may produce higher Q for lower input energy. Fig. 11 shows the results from one set of runs for classical diffusion with an initial cavity radius of 0.25 cm, and an outer radius of r_{max} = 1.0 cm. No runs were made for initial densities between 5×10^{21} and 1.0×10^{22} so the straight lines in this region simply indicate insufficient data.
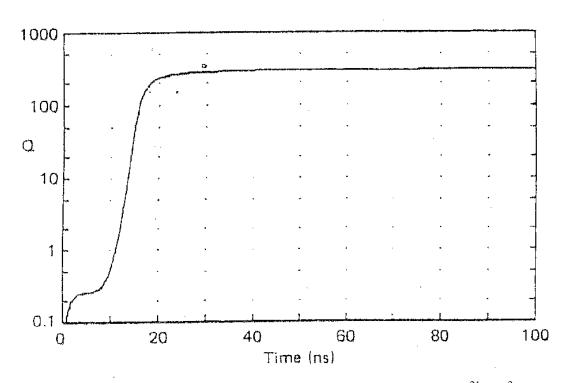
Fig. 8: Gain Q vs. Time for $E_{in} = 4.033$ MJ. B = 100 T, N = 5×10^{21} cm^{-3},
$T_o = 20$ keV, Classical Diffusion

4.0   Application to Propulsion

To assess the effectiveness of MICF as a propulsion system, we choose a pellet design such as that given in Fig. 5, namely one with $r_o = 0.15$ cm, $r_f = 0.18$ cm, and r_{max} 0.6 cm. We envisage a propulsion system as depicted in Fig. 12 where MICF pellets are injected into a reactor chamber where they are zapped by a beam of antiprotons $(\bar{p})$ and exhausted from the chamber via a magnetic nozzle which is an integral part of an external magnetic field that also serves to cushion the chamber walls from the shock of the microexplosions. We choose a modest rep rate (ω) of 10 Hertz so that the thrust produced by the system can be written as

$$F = \omega m_T v_e \qquad (69)$$

where m_T is the mass of the pellet and v_e the exhaust velocity of the pellet as it emerges from the nozzle, which occurs at the end of the burn. At that point (i.e., when the shock wave within the pellet has reached the outer metal surface), physical integrity of the pellet is no longer preserved and disassembly might take place, i.e., the pellet would perhaps be a collection of debris, but for simplicity we assume that the pellet remains intact as it comes out of the nozzle. In order to calculate v_e, we must first determine the energy content of the pellet at the end of the burn. We assume the "modified Bohm"
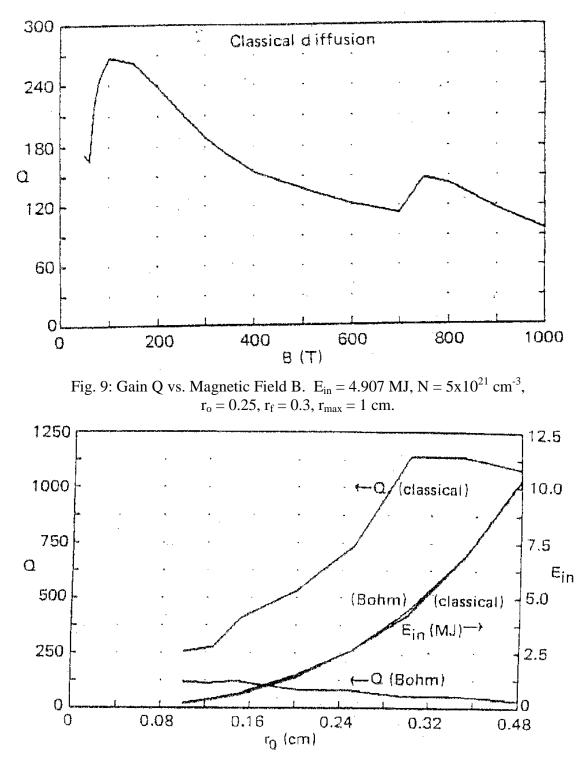
28

Fig. 9: Gain Q vs. Magnetic Field B. E_{in} = 4.907 MJ, N = 5×10^{21} cm^{-3},
r_o = 0.25, r_f = 0.3, r_{max} = 1 cm.

Fig. 10: Cut-off Input Energy E_{in} and Gain Q vs. Initial Cavity Radius r_o.
B = 100 T, N_o = 5×10^{21} cm^{-3}.

diffusion during the burn and, if we apply that scaling to the pellet in question, we find
that at E_{in} of 2 MJ the Q-value is about 900, giving an energy output of 1800 MJ. For the

pellet in question, the mass can be readily calculated to be 3.42 gm, and this yields $v_e = 1.03 \times 10^6 \, \frac{m}{s}$. This, of course, gives rise to $I_{sp} \approx 1.03 \times 10^5$ s which is well within the range displayed in Fig. 1. From Eq. (69), we find that the thrust generated by the system at $\omega = 10$ to be $F = 3.523 \times 10^4$ N.

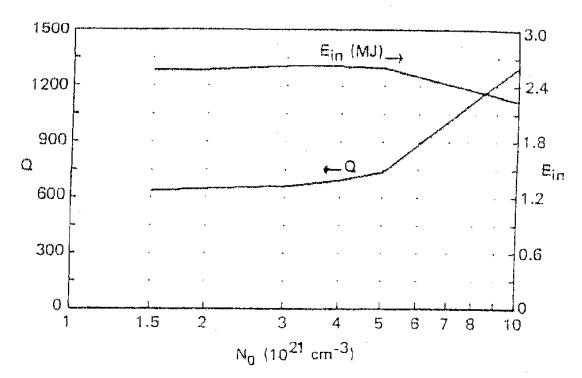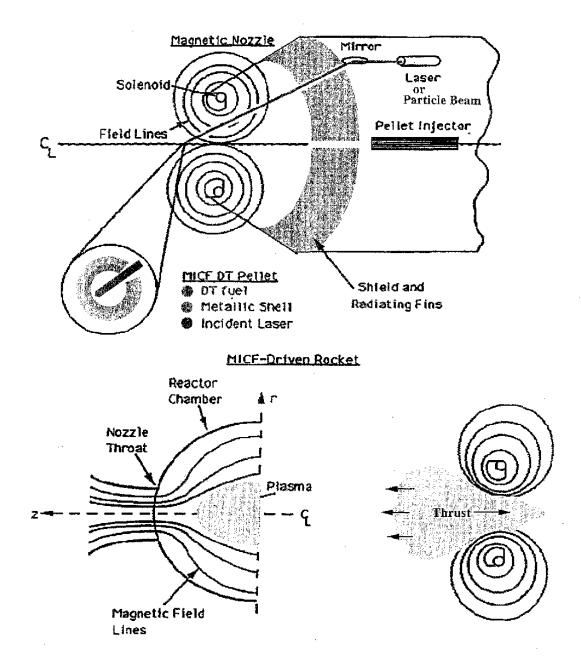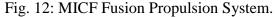Fig. 11: Cut-off Input Energy E_{in} and Gain Q vs. Initial Plasma Density N_o. B = 100 T, Initial cavity radius $r_o = 0.25$ cm.

As a first application to the MICF propulsion, we consider the one-way robotic mission to the Oort Cloud at 10,000 AU, a mission considered by NASA as a precursor to a mission to the nearest star, Alpha Centauri. From the standard non-relativistic rocket equation, it can be shown for a fly-by mission that the travel time t_f, and the distance s_f are given by[15]

$$t_f = \frac{m_i - m_f}{F} v_e \qquad (70)$$

$$s_f = \frac{m_i v_e^2}{F} \left[1 - \frac{m_f}{m_i} + \frac{m_f}{m_i} \ln \left(\frac{m_f}{m_i} \right) \right] \qquad (71)$$

Fig. 12: MICF Fusion Propulsion System.

$$v_f = v_e \ln \left[\cfrac{1}{1 - \dfrac{Ft_f}{m_i v_e}} \right] \qquad (72)$$

where m_i and m_f are the initial and final (dry) vehicle masses respectively, and v_f the velocity of the vehicle when it reaches its destination assuming it started from rest. Some design of the propulsion system is required in order to make use of the above equations

and for that we choose a design for a laser-driven inertial fusion rocket[16] but without the laser driver. The assumption being that an antiproton-driven system will be significantly less massive than a laser-driven one, and as a result, we estimate the dry mass of the vehicle to be 220 metric tons (mT). Clearly, this aspect of the analysis is subject to further investigation and detailed study which is beyond the scope of this work. Nonetheless, this choice of m_f appears to be reasonable and would allow a meaningful assessment of MICF as a propulsion system. Substituting these quantities into Eqs. (70) and (71), we find that the fly-by mission to 10,000 AU takes 47 years with the pellet design described above, and requires 166 gms of antiprotons to accomplish such a mission. Clearly, a more optimum design might yield significantly better results!

For the second propulsion example, we consider a round trip mission to Jupiter, a somewhat distant planet in the solar system. Using a continuous burn acceleration / deceleration type of trajectory at constant thrust, the travel time is given by Eq. (1) or

$$\tau_{RT} = \frac{4D}{v_e} + 4\sqrt{\frac{Dm_f}{F}} \tag{73}$$

where, in this case, D denotes the linear distance from Earth to Jupiter which is 6.29×10^{11} m. When the values of v_e, m_f, and F given earlier are inserted in this equation, the result is 120 days, and the amount of antiprotons required is 1.16 gm.

5.0   References

1. T. Kammash, Fusion Energy in Space Propulsion, AIAA Progress in Astronautics and Aeronautics, Vol. 167, Ch. 1 (1995).
2. D. J. Poston and T. Kammash, Nuclear Science and Engineering, 122, 55 (1996).
3. L. Spitzer, Jr., Physics of Fully Ionized Gases, Interscience Publishers, Inc., New York (1956).
4. Y. B. Zeldovich, and Y. P. Raizer, in Physics of Shock Waves and Hydrodynamic Phenomena, Academic Press, New York, p. 258 (1966).
5. C. A. Rouse, in Progress in High Temperature Physics and Chemistry, Vol. 4, p. 145, Pergamon Press (1971).
6. D. L. Galbraith and T. Kammash, Electric Power Research Institute Report EPRI-ER-521 (1978).
7. S. L. Greene, Lawrence Livermore National Laboratory Report UCRL-70522 (1967).
8. T. Kammash, Fusion Reactor Physics – Principles and Technology, Ann Arbor Science Publishers, Ch. 3 (1975).
9. T. Kammash and D. L. Galbraith, Nuclear Fusion, 13, 133 (1973).
10. D. L. Galbraith and T. Kammash, Fusion Technology, 16, 65 (1989).
11. N. A. Krall and A. W. Trivelpiece, Principles of Plasma Physics McGraw-Hill, New York, p. 20, (1973).
12. A. Hasegawa, et al, Nuclear Fusion, 28, 369 (1988).
13. A. Y. Aydemir, et al, Physics of Fluids, 30, 3038 (1987).
14. A. E. Mikhailovski, Soviet Physics, Doklady, 15, 471 (1970).
15. B. N. Cassenti and T. Kammash, STAIF 1999 CD-ROM (1999).

16. R. A. Hyde, Lawrence Livermore National Laboratory Report UCRL-88857 (1983).

6.0 Acknowledgments